Elemental analysis of rice using laser-ablation sampling: Determination of rice-polishing degree

Yonghoon Lee★

Department of Chemistry, Mokpo National University, 1666 Yeongsan-ro, Jeonnam 58554, Korea
(Received May 10, 2023; Revised June 19, 2023; Accepted June 21, 2023)

Abstract: In this study, laser-induced breakdown spectroscopy (LIBS) was used to estimate the degree of rice polishing. As-threshed rice seeds were dehusked and polished for different times, and the resulting grains were analyzed using LIBS. Various atomic, ionic, and molecular emissions were identified in the LIBS spectra. Their correlation with the amount of polished-off matter was investigated. Na I and Rb I emission line intensities showed linear sensitivity in the widest range of polished-off-matter amount. Thus, univariate models based on those lines were developed to predict the weight percent of polished-off matter and showed 3-5 % accuracy performances. Partial least squares-regression (PLS-R) was also applied to develop a multivariate model using Si I, Mg I, Ca I, Na I, K I, and Rb I emission lines. It outperformed the univariate models in prediction accuracy (2 %). Our results suggest that LIBS can be a reliable tool for authenticating the degree of rice polishing, which is closed related to nutrition, shelf life, appearance, and commercial value of rice products.

Key words: laser ablation, elemental analysis, rice polishing, laser-induced breakdown spectroscopy, multivariate modeling

1. Introduction

Recently, laser ablation has attracted much attention as an alternative sampling method in combination with elemental analysis techniques such as laser-induced breakdown spectroscopy (LIBS), inductively-coupled plasma optical emission spectroscopy (ICP-OES), inductively-coupled plasma mass spectrometry (ICP-MS) and other absorption- or fluorescence-based techniques.[1-3] Laser ablation atomizes solid materials by focusing a pulsed laser beam on the sample surface. Thus, complicated acid digestion and the following

dilution with a large factor can be removed from the sample preparation process. LIBS is the simplest laser-ablation-based elemental analysis technique.[4,5] In typical LIBS analysis in which a nanosecond pulsed laser is employed as an ablation source, the pulse energy in the range from a few to hundreds millijoules is focused into the area of $\sim 10^4$ mm^2 on the sample surface. A part of the laser pulse energy is used to heat the solid material or to break the chemical bonds among the atoms in the local area, and the vaporized (or ablated) atoms are further ionized to form a plasma. The other part of the laser

★ Corresponding author
Phone : +82-(0)61-450-2332　　Fax : +82-(0)61-450-2339
E-mail : yhlee@mokpo.ac.kr

pulse energy is absorbed by the emerging plasma in the nanosecond laser pulse duration (~10 ns).[6] The laser-induced plasma is an expanding, transient matter with a lifetime around a few tens of microseconds. It is composed of high-energy particles of ions, electrons, atoms, and small molecules. Eventually, the ions are combined with electrons to form atoms, and the atoms combine with each other to produce small molecules such as CN, C_2, oxides, fluorides, and chlorides depending on the elemental compositions of samples and ambient gas.[7-12] The laser-induced plasma dissipates its energy by emitting lights, sounds, and heats. LIBS performs quantitative or qualitative elemental analysis by recording the wavelength dispersed optical emissions from the laser-induced plasma. Typical temperature of laser-induced plasmas is ~10,000 K. Generally, LIBS shows parts-per-million-level detection capabilities for most elements in the periodic table for the use of quantitative analysis techniques.[13] However, LIBS has various analytical applications other than quantitative analysis. It can quickly identify the major elements in a sample material, classify or discriminate particular samples, and make a map of elemental distribution to locate defects.[14-16]

Rice has been produced and consumed as staple food mainly in Asian countries.[17] Recently, significant amount of rice is also produced in African and American counties such as Nigeria, Madagascar, and United States.[18] LIBS has been used for rice analysis for several applications. Kim et al. reported feasibility of LIBS for quantitative analysis of nutrient elements such as Mg, Ca, Na, and K at the limit-of-detection (LOD) level of a few parts per millions.[19] As well as the nutrient elements, LIBS was applied to analyze the elements of concern for food safety such as Cu, Cd, and Pb in combination with multivariate calibration, sample phase transformation, and electro-chemical preconcentration.[20-22] Sharma et al. investigated difference in molecular and elemental composition between the rice products infected by false smut disease and healthy ones using Fourier-transform infrared (FT-IR) spectroscopy, wavelength-dispersed X-ray fluorescence (XRF), and LIBS.[23] Kim et al.

could differentiate pesticide-contaminated and pesticide-free rice products based on LIBS spectra.[19] However, the majority of researches has been devoted to the investigation of LIBS performances in authentication or classification of rice products. LIBS spectra were successfully used for modeling not only geographic but also botanic origins of rice.[24-28] Various chemometric algorithms such as support vector machine (SVM), linear discriminant analysis (LDA), k-nearest neighbors (k-NN), random forest (RF), decision tree (DF), partial least squares-discriminant analysis (PLS-DA), and artificial neural network (ANN) were employed for those works.

Rice grains are covered by a fibrous, inedible outer layer called the hull or husk. Removing this outer layer from rice seeds is an important step in processing rice for human consumption. The rice dehusking or further polishing is generally conducted to improve digestibility, remove impurities, increase shelf-life, and make rice grains smooth and white. However, dehusked and further polished rice grains, so called white rice, have lower nutritional contents than those of brown rice because more than 60 % of nutrients is concentrated in rice kernel located in the outer part of a whole grain. Inorganic elements are also populated more in the outer part of a rice grain.[29-31] Thus, as the dehusking and polishing processes are conducted further and further, carbohydrates in the remaining grains become dominant. Under this circumstance, a compromise among nutritional contents, shelf-life, and other benefits of extensive polishing can be one of the important factors to be considered to provide better rice products. Therefore, a rapid reliable technique that estimates rice dehusking or polishing degrees would be very helpful for controlling the rice polishing process and assessing rice quality considering nutrition, shelf-life, aesthetics, and other factors.

Herein, we report a novel application of LIBS as a reliable technique for estimating the degree of rice polishing. Rice seed samples were dehusked and polished for several different times. Then, the resulting grains were milled and pelletized for LIBS analysis. Atomic or ionic emission lines of C, Si, Mg, Ca, Mn, Na, H, Li, N, K, O, and Rb and molecular emissions
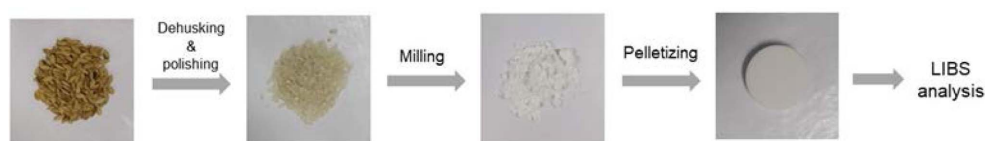
Fig. 1. Sample preparation scheme for LIBS analysis.

of CN were identified in their LIBS spectra. The correlation of those intensities with the amount of polished-off matter was investigated and revealed the inhomogeneous distributions of those elements in the rice seeds. The Na I emission line at 589.592 nm and the Rb I emission line at 780.027 nm showed linear sensitivity in the widest range of the polished-off-matter amount, although there was found a discontinuity in emission line intensities due to matrix difference between husks and grains. Thus, univariate models (linear fits) based on the intensities of the Na I and Rb I emissions were developed and applied to predict the weight percent of the polished-off matter. Multivariate modeling of the polished-off-matter amounts was also performed using PLS-R. For the PLS-R modeling, Si I, Mg I, Ca I, Na I, K I, and Rb I emission line intensities were used as predictor variables. The multivariate model was found to be more accurate than the univariate ones in predicting the polished-off-matter amounts. For the rice grains, the polished-off-matter amount could be predicted accurately within ~2 wt% by the multivariate model. Moreover, PLS-R was found to show a dependable performance in modeling and predicting the polished-off-matter amounts including unhusked rice seed samples. Consequently, LIBS calibrated appropriately can be employed as a dependable technique for estimating the degree of rice polishing.

2. Experimental

2.1. Sample preparation

A bag of short-grain rice (40 kg) grown in Gyeongnam, Republic of Korea was purchased for this work. The rice seeds were polished for the nine different times, 5, 10, 15, 20, 25, 30, 35, 40, and 45 minutes, using a home rice polishing machine (Baro Tech, Gimpo, Republic of Korea). A 20 g of each polished grain sample was taken and put in an agata vial with two agata balls. Then, the grain sample was milled for 30 minutes using a ball mill (8000M Mixer/Mill, SPEX SamplePrep). The milled powder was pressed into a pellet using a hydraulic press (CrushIR™, PIKE Technologies). A 5 g of each milled sample powder was placed in a 13 mm stainless-steel die and pressed under 10 tons for 5 minutes. The sample preparation process is presented in *Fig.* 1.

2.2. LIBS analysis

To conduct LIBS measurements, a commercial instrument (RT100-EC, Applied Spectra, Inc.) was utilized, which consisted of a flash-lamp-pumped Q-switched Nd:YAG laser (POLARIS II, New Wave Research) and a 6-channel spectrometer equipped with charge-coupled device (CCD) detectors. A fundamental beam from the Nd:YAG laser at the wavelength of 1064 nm was directed and focused onto the sample surface, with a laser beam spot size of 75 μm in diameter. The laser pulse energy and the repetition rate were 10 mJ/pulse and 10 Hz, respectively. The spectrometer covered from 180 nm to 890 nm, and its resolution was approximately 0.1 nm. The CCD detection gate delay from the laser pulse was set to 0.5 μs, and the optical emission signal was integrated for 1.05 ms. For each sample pellet, 25 line scans were conducted. The length of each scan line was 8 mm. For the line scan, the sample was translated at the rate of 1 mm/s. Thus, 80 laser pulses were launched in a 8-mm line on the sample pellet surface, and the 80 single-shot optical emissions were accumulated for recording a LIBS spectrum. Two nearby scan lines were separated by 250 micrometer.

3. Results and Discussion

3.1. Estimation of polished-off-matter amount

The rice seeds were dehusked and polished using a home rice polishing machine. Setting the polishing time to 5 minutes, a 500 g of rice grains were polished once. In *Fig.* 2(a), the images of as-threshed rice seeds (S0), and polished rice grains (from S1 to S9). After the five-minute polishing, the grains denoted as S1 were obtained. Another 500 g of rice seeds were polished for 10 minutes. The resulting grains (S2) are shown in *Fig.* 2(a). For separate seven more 500 g of rice seeds, the polishing processes were conducted for 15, 20, 25, …, and 45 minutes. The
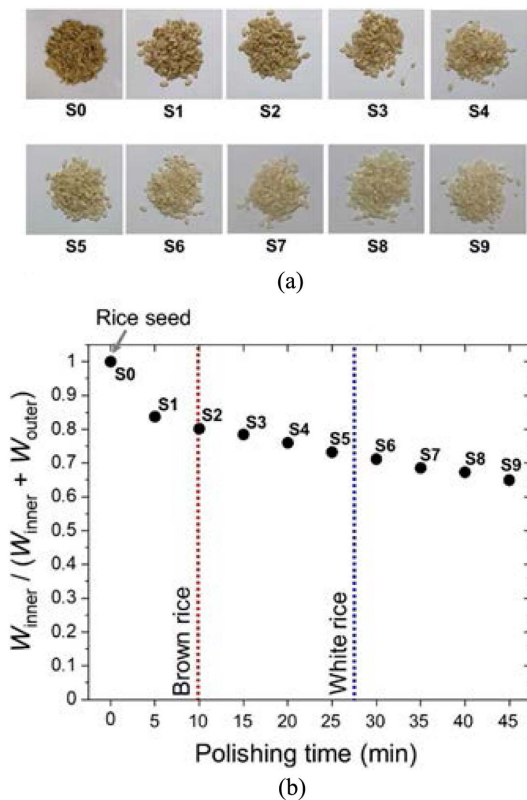

(a)

(b)

Fig. 2. (a) Images of rice seeds (S0) and grains polished for 5 – 45 minutes (from S1 to S9) using a home rice polishing machine and (b) the ratios of the remaining grain mass, W_{inner}, to the total mass, $W_{inner} + W_{outer}$, with respect to the polishing time. In b, the vertical red and blue dotted lines indicate the mass ratios corresponding to brown rice (0.80) and white rice (0.72), respectively.

resulting grains were also shown in *Fig.* 2(a) (see the grains denoted as "S3", "S4", "S5", …, and "S9", respectively). The ratio of the remaining grain weight to the total grain weight after the polishing process is defined as $W_{inner} / (W_{inner} + W_{outer})$. W_{inner} and W_{outer} are the weight of the remaining grains and that of the polished-off matter, respectively. The polished-off part is actually the outer part of rice seeds. In *Fig.* 2(b), the ratio, $W_{inner} / (W_{inner} + W_{outer})$, is plotted with respect to the polishing time. Generally, rice bran occupies 20 % of an as-threshed rice seed in weight. Thus, in South Korea, the rice grains with $W_{inner} / (W_{inner} + W_{outer}) = 0.80$ are circulated in markets as a commercial minimally-processed brown rice which corresponds to the rice grains polished for 10 minutes in this experiment (see the grains denoted as "S2" in *Fig.* 2(a) and the vertical red dotted line for brown rice in *Fig.* 2(b)). Brown rice grains contain almost the whole part of germs. This makes brown rice more nutritional than white rice. When a 10 % of weight is polished off from the outer part in brown rice, the germs are completed removed. In this case, the corresponding mass ratio, $W_{inner} / (W_{inner} + W_{outer})$, is 0.72, and this is marked by the vertical blue dotted line in *Fig.* 2(b). It should be noted that the change in $W_{inner} / (W_{inner} + W_{outer})$ from S0 to S1 is remarkably larger than the others. This indicates that most of husks, which are softer than grains, were removed from rice seeds within 5 minutes.

3.2. Intensity variations with polished-off-matter amount

Fig. 3 shows LIBS spectra of the rice seeds (S0), the husks obtained after the 5-min polishing, and the grains obtained after 45-min polishing (S9). The husks show richer, stronger emission lines than the rice seeds and the grains. Thus, the identified atomic and ionic emission lines were denoted along the LIBS spectrum of the husk sample. These assignments were conducted based on the NIST Atomic Spectra Database.[32] As shown in *Fig.* 3, atomic or ionic emission lines of C, Si, Mg, Ca, Mn, Na, H, Li, N, K, O, and Rb and molecular emissions of CN were identified in the LIBS spectra. According to the

United States Department of Agriculture (USDA) Database, in dried short-grain rice, carbohydrates are the major component (91.3 wt%) and the second and third most abundant nutrients are proteins (7.5 wt%) and fats (0.6 wt%), respectively.[33] Thus, the matrix element can be identified as C and its atomic emissions at 193.091 nm and 247.856 nm are observed in the LIBS spectra. Also, the CN molecular emission band around 385 nm can be attributed to combination of C ablated from the sample and N from N_2 in ambient air.[34,35] Among metallic elements, K (830 mg/kg), Mg (250 mg/kg), and Ca (32 mg/kg) are the three most abundant elements in the dried short-grain rice at the parts-per-million level. They are well discernible in the LIBS spectra shown in *Fig.* 3.

For selected emission lines, their intensity variations with the degree of rice polishing were investigated. The degree of rice polishing, D, is defined as the following equation:

$$D = \frac{W_{outer}}{W_{inner} + W_{outer}} \quad (1)$$

This is the weight ratio of polished-off matter (W_{outer}) to the rice seeds ($W_{inner} + W_{outer}$). Among the emission lines assigned in *Fig.* 3 (see the panel in the middle), those at 247.856 nm (C I), 288.158 nm (Si I), 518.360 nm (Mg I), 616.217 nm (Ca I), 589.592 nm (Na I), 769.896 nm (K I), and 780. 027 nm (K I) were chosen for the investigation of intensity variation. The spectroscopic parameters of these selected emission lines are listed in *Table* 1. In the cases of Mg, Ca, Na, and K, there are stronger emission
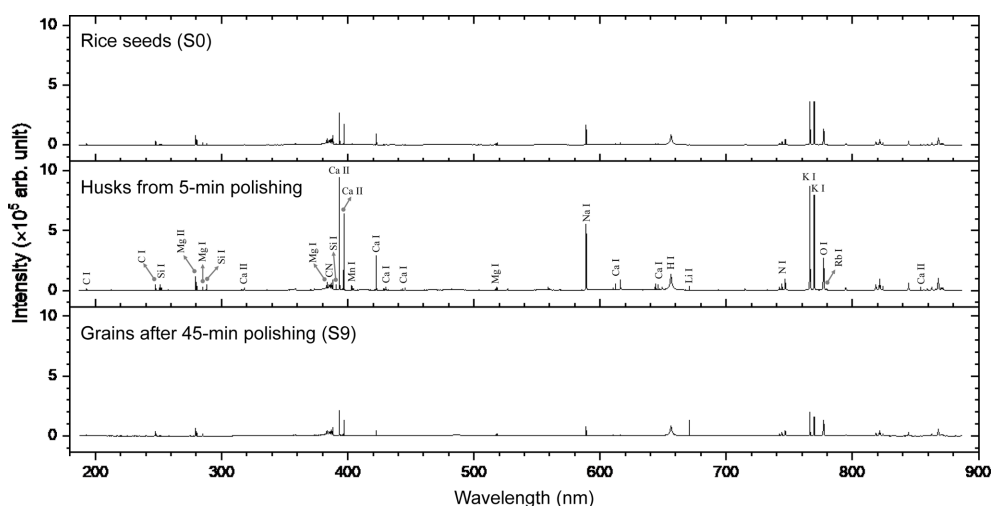

Fig. 3. LIBS spectra of rice seeds, S0, (top), husk obtained from 5-min polishing (middle), and grains remaining after 45-min polishing, S9, (bottom).

Table 1. Spectroscopic parameters of atomic and ionic emission lines selected for analysis. A_{ki}, E_i, E_k, g_i, and g_k are the spontaneous emission coefficient, the lower-level energy, the upper-level energy, the lower-level statistical weight, and the upper-level statistical weight, respectively

Species	Wavelength (nm)	A_{ki} (s^{-1})	E_i (cm^{-1})	E_k (cm^{-1})	g_i	g_k
C I	247.856	2.8×10^7	21648.03	61981.83	1	3
Si I	288.158	2.17×10^8	6298.85	40991.88	5	3
Mg I	518.360	5.61×10^7	21911.18	41197.40	5	3
Ca I	616.217	4.77×10^7	15315.94	31539.50	5	3
Na I	589.592	6.14×10^7	0.00	16973.37	2	2
K I	769.896	3.734×10^7	0.00	12985.19	2	2
Rb I	780.027	3.812×10^7	0.00	12816.55	2	4

lines than those selected, but the weaker selected lines show the better sensitivity to D. For example, there are strong emission lines of Ca at 393.366, 396.847 and 422.673 nm.[32] When the limit-of-detection performance is important, employing the stronger emission lines would be reasonable. However, the weaker line at 616.217 nm was selected herein because the better sensitivity of emission intensity with D could be obtained with the weaker line. The better correlation of the intensity measured for the weaker emission line with concentration (or concentration dependent parameter such as D) is frequently observed

in LIBS-based calibration curves and attributed to the effect of self-absorption, which becomes more significant with stronger emission lines.[5] Thus, the weaker lines were used to investigate their intensity variation. In *Fig.* 4(a), intensity values of the C I emission line at 247.856 nm was plotted as a function of D. Each 25 spectra recorded per pellet sample shows a relative standard deviation (RSD) of ~4% for the C I line intensity at 247.856 nm, and the ten samples from S0 to S9 show an agreement of the C I line intensity within 6 % in terms of RSD without any spectral intensity normalization to correct pellet-to-pellet intensity variation. Thus, it is confirmed that the emission line intensity of the matrix element, C, is almost constant over the rice samples polished in different times. However, the Si I line intensity at 288.158 nm varies differently from that of the C I line (see *Fig.* 4(b)). The S0 sample (rice seeds) shows the strong Si I line intensity in its LIBS spectra, but the intensity drastically decreases as the polishing time increases (see *Fig.* 3(b)). This indicates that most of Si is contained in the rice husks. Therefore, Si emission lines observed in LIBS spectra can be used as variables indicating if husks are removed completely from rice seeds or not.

Fig. 5 shows (a) K I, (b) Mg I, (c) Ca I, (d) Na I, and (e) Rb I emission line intensity variations with D. Latent variables for univariate modeling of the degree of rice polishing were chosen in consideration of these intensity variations. Except for the S0 sample that includes husks, all of the emission lines measured for the grains show monotonous decreases from S1 to S9. The clear discontinuity between S0 and S1 can be attributed to difference in physical properties and chemical composition between husks and grains. The variations from S1 to S9 are consistent with the fact that most of the nutrients are populated in the outer parts of rice grains. To be used as effective variables for modeling the degree of rice polishing, the intensity of a promising emission line should vary monotonously showing one-to-one correspondence between intensity and D with enough sensitivity. In consideration of this requirement, the Na I emission line at 589.592 nm and the Rb I emission line at
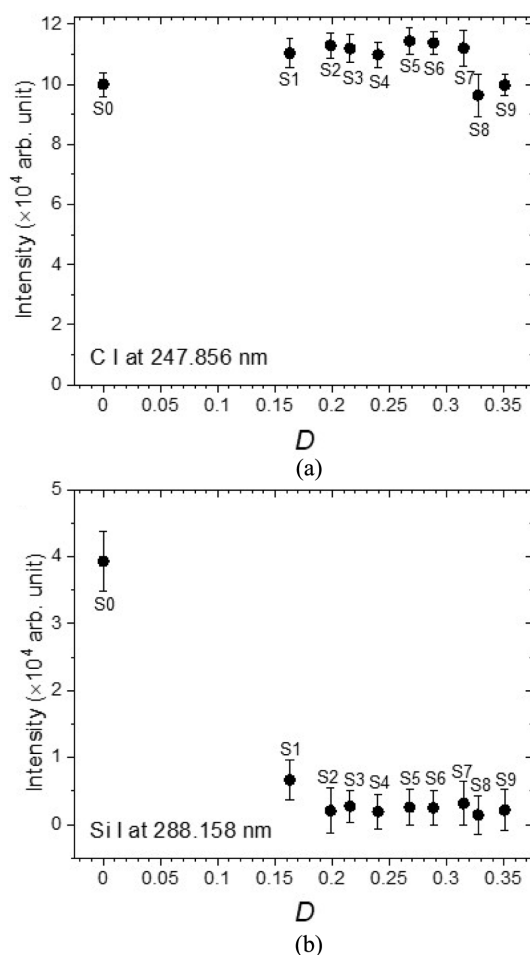

Fig. 4. Intensities of C I and Si I emission lines at 247.856 nm and 288.158 nm, respectively, with respect to the degree of rice polishing, $D = W_{outer} / (W_{inner} + W_{outer})$. Each data was labeled with its corresponding sample code.
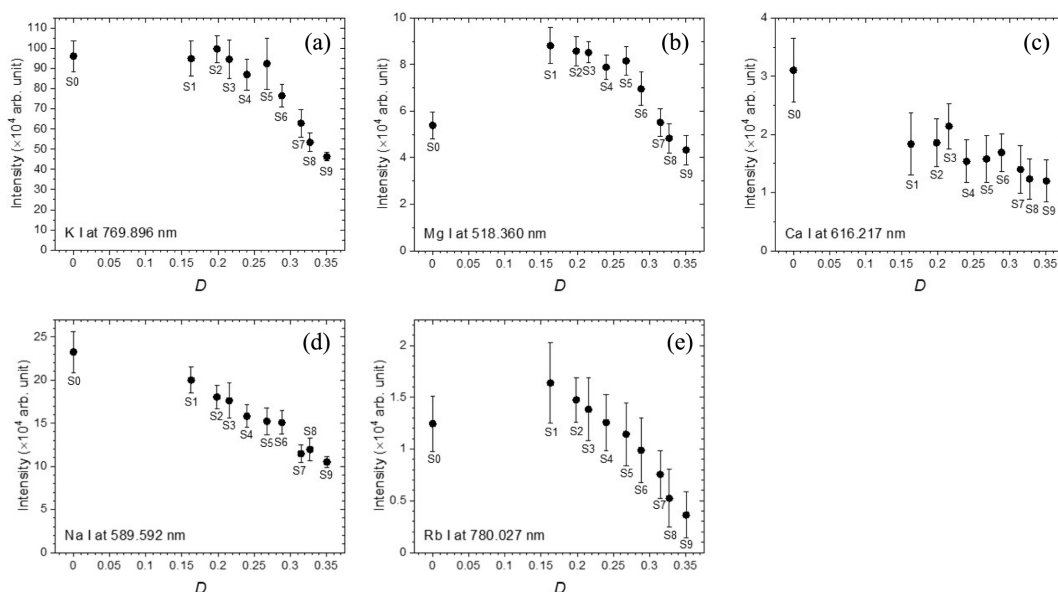
Fig. 5. Intensities of (a) K I, (b) Mg I, (c) Ca I, (d) Na I, and (e) Rb I emission lines with respect to the degree of rice polishing, $D = W_{\text{outer}} / (W_{\text{inner}} + W_{\text{outer}})$. Each data was labeled with its corresponding sample code.

780.072 nm were selected for univariate models to predict the degree of rice polishing. In cases of the K I emission line at 769.896 nm and the Mg I emission line at 518.360 nm, the corresponding sensitivity from $D = 0.16$ (S1) to 0.27 (S5) is too low to distinguish the samples, S1, S2, S3, S4, and S5. Also, the sensitivity of the Ca I emission line at 616.217 even looks worse than those of the K I and Mg I emission lines.

3.3. Univariate modeling of polished-off-matter amount

As mentioned above, 25 LIBS spectra were recorded per sample. Univariate models were developed with the nine samples (S1 – S9). The rice seed sample (S0) was excluded due to the severe discontinuity observed between the data of S0 and S1. Thus, totally, 225 (= 25 data × 9 samples) data were used for the univariate models. The 225 data were separated into two sets for model calibration and validation. For the calibration dataset, 13 data from each sample's 25 data were randomly selected and included to form the dataset with 117 (= 13 data × 9 samples) data. The remaining 12 data of each sample were included in the validation dataset with 108 (= 12 data × 9

samples) data. Then, the univariate models based on Na I and Rb I emission line intensities were developed using the calibration dataset, and the performance of these models were validated using the validation dataset. The accuracy performances in terms of root-mean-square error of prediction (RMSEP) were estimated from the validation processes.

Fig. 6 shows the univariate models, which are linear fits of the experimental data. The two linear fits obtained using Na I and Rb I emission line intensities in the calibration datasets are represented by the solid red lines in *Figs.* 6(a) and 6(b), respectively. The fitted parameters, offsets and slopes, are noted in the corresponding panels. Although RSD of the Rb I emission intensities obtained for each sample looks larger than that of the Na I emission line, the linear fit well describes the intensity variation with D. To evaluate accuracy performances of the univariate models, RMSEP values were obtained using the separate validation datasets. The RMSEP values were calculated by the following equation:

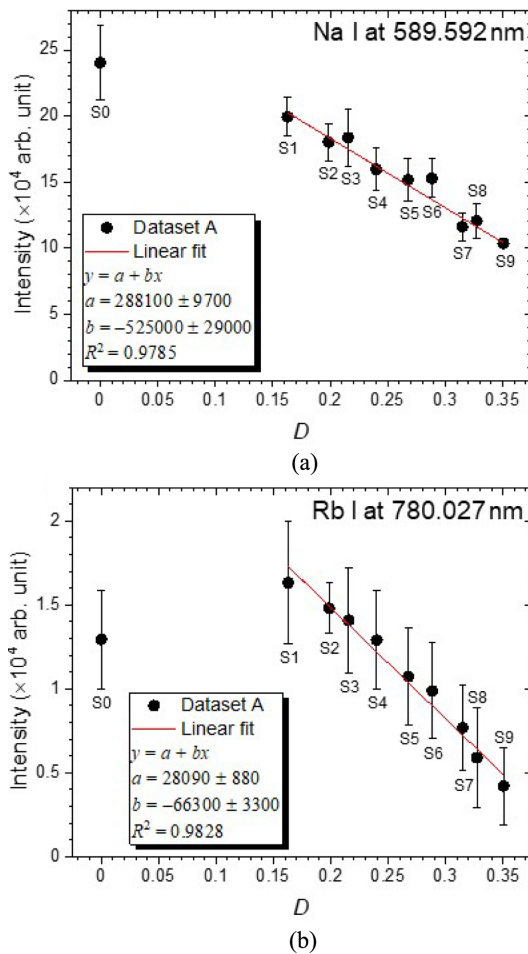$$RMSEP = \sqrt{\frac{\sum_{i=1}^{n}(D_i^{Pred} - D_i^{ref})^2}{n}} \qquad (2)$$

Fig. 6. Univariate calibration models (linear fits) based the emission line intensities of (a) Na I at 589.592 nm and of (b) Rb I at 780.027 nm. Each experimental data was labeled with its corresponding sample code.

In the equation, D_i^{pred} and D_i^{ref} are predicted and reference degree of rice polishing that correspond to the ith test data, and n is the number of data in the validation dataset. Herein, the number of data in the validation dataset, n, is 108. The RMSEP values are listed in Table 2. The univariate models based on the

Na I emission line gave RMSEP values about 0.03; RMSEP of the model calibrated by the dataset A and tested by the dataset B is 0.027, and switching the test dataset, RMSEP is slightly increased to 0.032. The models based on the Rb I emission line are found to be inferior to that based on the Na I emission line in accuracy performance; in the two validation processes with switched calibration and test datasets, both RMSEP values are larger than those of the Na I-based models. This can be rationalized by the larger RSD (or the weaker intensity) of the Rb I emission line than that of Na I.

3.4. Multivariate modeling of polished-off-matter amount

PLS-R is a statistical technique used for modeling the relationship between a set of predictor X variables and one or more response Y variables.[36] Herein, the predictor variables are the emission intensities of the selected lines, and the response is D. With the singe response variable given in this work, PLS-R worked by finding latent variables, also known as PLS factors that explain the variance in D. In consideration of the discontinuity in D between S0 and the others, PLS-R modeling was performed with S1 - S9, first.

Fig. 7 shows the results from PLS-R modeling of S1 - S9. For this modeling, Si I, Mg I, Ca I, Na I, K I, and Rb I line emission intensities were used as X variables. That of C I was not used because the C I emission intensity was found not to be correlated with D (see Fig. 4(a)). In Fig. 7(a), the explained Y-variance was plotted as a function of the number of PLS factors used in the PLS-R modeling. It shows the first PLS factor explains 72.6 % of the Y-variance and when the second factor explaining 12.0 % of the Y-variance is included the model exploits 84.6% of the Y-variance. The minor ones, PLS factors 3, 4, 5,

Table 2. RMSEP values of univariate and multivariate models obtained from the validation

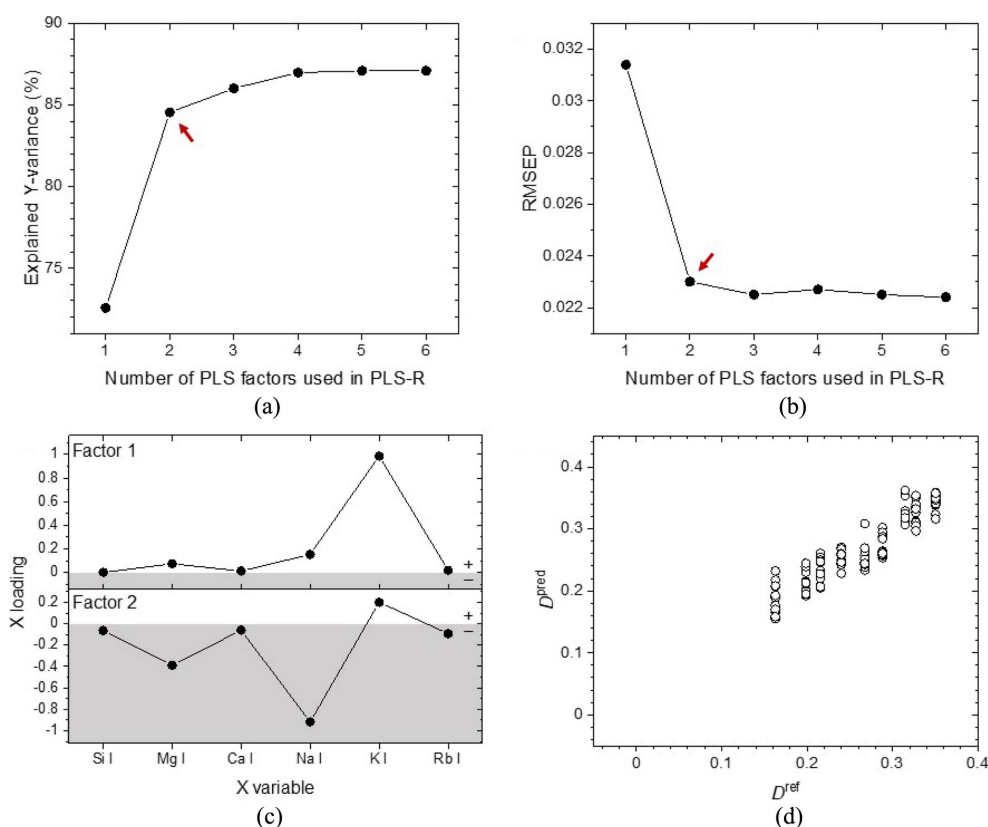|	Model	Samples	RMSEP
Univariate	Na I	S1 − S9	0.027
(Linear fit)	Rb I	S1 − S9	0.046
Multivariate	Si I, Mg I, Ca I, Na I, K I, Rb I	S1 − S9	0.023
(PLS-R)	Si I, Mg I, Ca I, Na I, K I, Rb I	S0 − S9	0.029

Fig. 7. (a) Explained Y-variance from calibration of the PLS-R model, (b) RMSEP from validation of the model, (c) X-loadings of PLS factors 1 and 2, and (d) correlation between D^{ref} and D^{pred} from validation of the model using PLS factors 1 and 2. These results were obtained by modeling the S1 − S9 samples. The explained Y-variance and the RMSEP value from the model using the first two major PLS factors are indicated by the arrows in a and b, respectively. In c, positive and negative loadings are differentiated by the background colors, white and gray for positive (+) and negative (−), respectively.

…, do not make significant contribution to explanation of the Y-structure. Thus, it is reasonable to employ PLS factors 1 and 2 for modeling. This is consistent with the observation of RMSEPs shown in *Fig*. 7(b), where the RMSEP values, calculated using the above Eq. (2), are plotted with respect to the number of PLS factors used for modeling. The RMSEP was decreased remarkably by employing the two major PLS factors 1 and 2 for modeling as indicated by the arrow in *Fig*. 7(b), and the additional ones, however, made no significant decrease in RMSEP. As a result, the major two PLS factors were found to be enough for modeling D values of S1-S9.

The loadings of the selected-emission-line intensities to the PLS factors 1 and 2 are shown in *Fig*. 7(c).

The loadings have positive or negative values because PLS factors are extracted from the mean-centered data. The positive and negative loadings are differentiated by the background colors, white (+) and gray (−), respectively, in *Fig*. 7(c). The PLS factor 1 is dominated by the K I emission line intensity because it shows the largest variation with D among the selected emission lines (compare the intensity scales of the plots shown in *Figs*. 4(b) and 5(a)-5(e)). It indicates that the K I emission line intensity shows the most sensitive decrease with D, but the sensitivity varies only from S5 to S9. Thus, for a complete model, other features are necessary.

The PLS factor 2 shows a positive correlation, the same signs (−) of the loadings, between Mg I and Na

I emission line intensities. This means that both Mg I and Na I emission line intensities behave alike as D decreases. Particularly, Na I is found to be able to supplement the effective sensitivity between S1 and S5 as well as for the others. The variations of Ca I and Rb I emission line intensities are smaller than those of K I, Na I, and Mg I (see the plots in *Fig.* 5). Thus, their loadings are also small in both PLS factors 1 and 2. In the case of Si I, its intensity appeared strongly only in the LIBS spectrum of the S0 sample which was excluded from modeling. The small loadings of the Si I emission line intensity in the PLS factors 1 and 2 can be understood in this way.

Fig. 7(d) shows the correlation between D^{ref} and D^{pred} obtained from validation of the PLS-R model

based on the two PLS factors 1 and 2. The corresponding RMSEP is 0.023, which indicates that the PLS-R model based using the two PLS factors outperforms the univariate models based on the Na I and Rb I emission line intensities in prediction accuracy (refer the RMSEPs listed in *Table* 2).

The PLS-R model's accuracy in predicting D including the S0 sample was also investigated. The results are shown in *Fig.* 8. To predict D from rice seeds, that is S0, the modeling was performed considering all S0-S9 samples. The explained Y-variance values was plotted as a function of the number of PLS factors used for the model in *Fig.* 8(a). The PLS factors 1, 2, and 3 explain 52.3 %, 30.0 %, and 5.6 % of the Y-variance, respectively, which
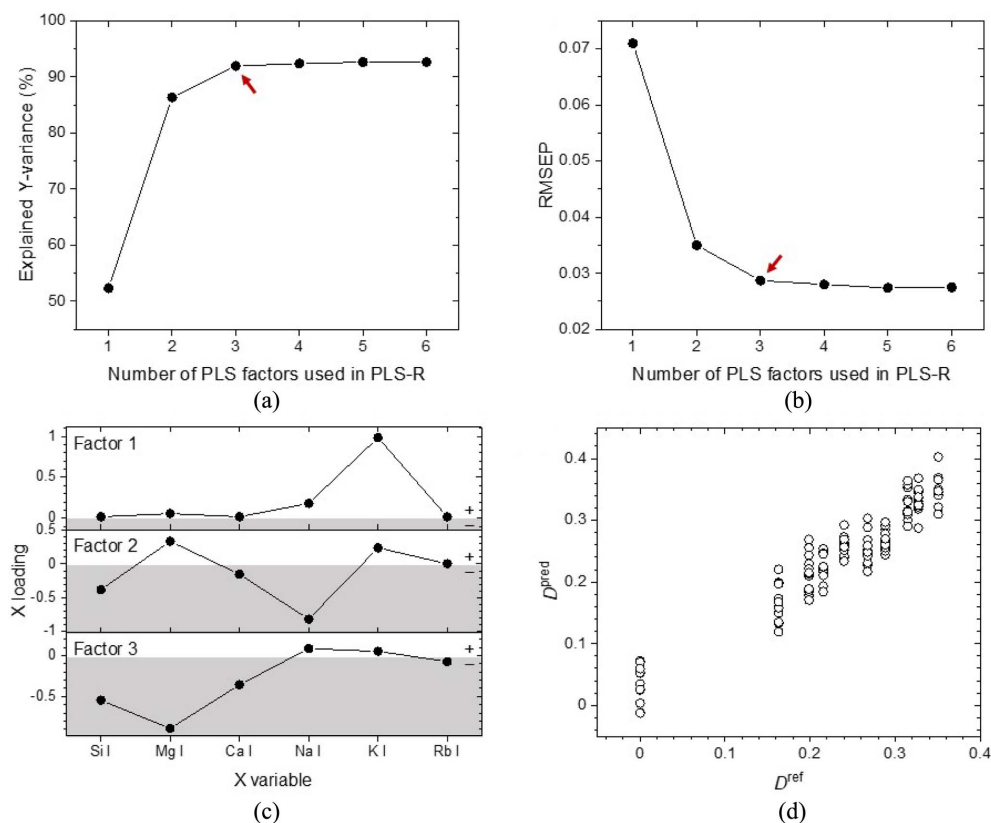

Fig. 8. (a) Explained Y-variance from calibration of the PLS-R model, (b) RMSEP from validation of the model, (c) X-loadings of PLS factors 1 − 3, and (d) correlation between D^{ref} and D^{pred} from validation of the model using PLS factors 1 − 3. These results were obtained by modeling the S0 − S9 samples. The explained Y-variance and the RMSEP value from the model using the first two major PLS factors are indicated by the arrows in a and b, respectively. In c, positive and negative loadings are differentiated by the background colors, white and gray for positive (+) and negative (−), respectively.

accumulates to 91.9 %. Each of the other factors explains less 0.2 % of the Y-variance. Thus, they can be ignored for modeling. This is consistent with the observation in the variation of RMSEP with the number of factors used in PLS-R modeling. The first three factors decrease RMSEP remarkably, as indicated by the arrow, and the following ones do very slightly (see *Fig*. 8(b)). Under this circumstance, including the PLS factors 4, 5, 6, … can lead to overfitted models. Considering explained Y-variance and RMSEP, the optimal number of PLS-R factors is found to be 3 (PLS factors 1-3). The loadings of PLS factors 1-3 are shown in *Fig*. 8(c). The loading of PLS factor 1 is dominated by the K I emission line intensity, as observed in modeling S1-S0 (see *Fig*. 7(c)). In PLS factors 2 and 3, Na I and Mg I emission line intensities are loaded, respectively, as major features. It should be noted that the Si I emission line intensity shows significant contributions to the PLS factors 2 and 3 unlike that in the modeling of S1-S9. This is due to inclusion of S0 of which LIBS spectrum shows strong Si I emission line intensities. The correlation between D^{ref} and D^{pred} is plotted in *Fig*. 8(d). This was obtained from the model developed using the three major PLS factors. The corresponding RMSEP is 0.029, as listed in *Table* 2.

4. Conclusions

To our knowledge, this work presents the first investigation into the feasibility of using LIBS as a reliable technique for bulk analysis of the rice-polishing degree. Using a typical LIBS system assembled with a nanosecond-pulsed laser and a multi-channel CCD spectrometer, the polished-off-matter amounts could be measured with the accuracy of ~2 % with the aid of multivariate PLS-R modeling. This modeling is based on the variation of elemental composition from periphery to inner grain of a rice seed. Although several emission lines showed intensity variations with the degree of rice polishing, the sensitivity of most emission lines was not linear in the enough range of the degree of rice polishing to cover rice seeds, brown rice grains, and white rice grains, together.

Among the seven emission lines of which intensity variations were investigated, those of Na I and Rb I provided dependable univariate models (linear fits) covering brown and white grains with accuracy of 3 -5 %. However, the multivariate PLS-R modeling, that took account of the emission lines of Si I, Mg I, Ca I, Na I, K I, and Rb I, outperformed the univariate models. This suggests that the sensitivity provided by those six elements is more or less complementary to one another. Also, the multivariate PLS-R provided a reliable model encompassing rice seeds and grains. Particularly, the Si I emission line was found to provide the sensitivity for the husks contained by rice seeds. Overall, our results indicate that LIBS combined with appropriate modeling approaches can be a useful bulk-analysis technique for assessing the degree of rice polishing which is an important factor closely related to nutritional contents, shelf life, price, and appearance of rice products.

Acknowledgements

References

1. R. E. Russo, X. Mao, J. J. Gonzalez, V. Zorba, and J. Yoo, *Anal. Chem.*, **85**(13), 6162-6177 (2013). https://doi.org/10.1021/ac4005327

2. J. Merten, *Spectrochim. Acta Part B: Atom. Spectrosc.*, **189**, 106358 (2022). https://doi.org/10.1016/j.sab.2022.106358

3. M. Miyabe, M. Kato, and S. Hasegawa, *J. Anal. At. Spectrom.*, **38**(2), 347-358 (2023). https://doi.org/10.1039/D2JA00304J

4. F. J. Fortes, J. Moros, P. Lucena, L. M. Cabalín, and J. J. Laserna, *Anal. Chem.*, **85**(2), 640-669 (2013). https://doi.org/10.1021/ac303220r

5. D. W. Hahn and N. Omenetto, *Appl. Spectrosc.*, **66**(4), 347-419 (2012). https://doi.org/10.1366/11-06574

6. J. P. Singh and S. N. Thakur, 'Laser-Induced Breakdown

Spectroscopy', 1st Ed., Elsevier Science B.V., 2007.

7. T. A. Alrebdi, A. Fayyaz, H. Asghar, S. Elaissi, and L. A. El Maati, *Molecules*, **27**(15), 5048 (2022). https://doi.org/10.3390/molecules27155048

8. V. F. Lebedev, M. K. Rabchinskii, M. S. Kozlyakov, D. N. Stepanov, A. V. Shvidchenko, N. V. Nikonorov, and A. Ya. Vul', *J. Anal. At. Spectrom.*, **33**(2), 240-250 (2018). https://doi.org/10.1039/C7JA00331E

9. A. K. Rai, J. K. Pati, C. G. Parigger, S. Dubey, A. K. Rai, B. Bhagabaty, A. C. Mazumdar, and K. Duorah, *Molecules*, **25**(4), 984 (2020). https://doi.org/10.3390/molecules25040984

10. E. J. Kautz, P. J. Skrodzki, M. Burger, B. E. Bernacki, I. Jovanovic, M. C. Pillips, and S. S. Harilal, *J. Anal. At. Spectrom.*, **34**(11), 2236-2243 (2019). https://doi.org/10.1039/C9JA00228F

11. M. Martinez, G. J. Harry, E. N. Haynes, Pi-I. D. Lin, E. Oken M. K. Horton, R. O. Wright, M. Arora, and C. Austin, *J. Anal. At. Spectrom.*, **38**(2), 303-314 (2022). https://doi.org/10.1039/D2JA00134A

12. L. J. Fernández-Menéndez, C. Méndez-López, C. Abad, J. Fandiño, C. González-Gago, J. Pisonero, and N. Bordel, *Spectrochim. Acta Part B: Atom. Spectrosc.*, **190**, 106390 (2022). https://doi.org/10.1016/j.sab.2022.106390

13. A. W. Miziolek, V. Palleschi, and I. Schechter, 'Laser-Induced Breakdown Spectroscopy (LIBS) Fundamentals and Applications', 1st Ed., Cambridge University Press, 2006.

14. H. Kim, J. Lee, E. Srivastava, S. Shin, S. Jeong, and E. Hwang, *Spectrochim. Acta Part B: Atom. Spectrosc.*, **184**, 106282 (2021). https://doi.org/10.1016/j.sab.2021.106282

15. L. Brunnbauer, Z. Gajarska, H. Lohninger, and A. Limbeck, *TrAC Trends Anal. Chem.*, **159**, 116859 (2023). https://doi.org/10.1016/j.trac.2022.116859

16. S. Jung, S. Kim, S. Kim, I. Park, Y. Moon, J.-H. Heo, S.-H. Nam, and Y. Lee, *Mater. Today Commun.*, **33**, 104867 (2022). https://doi.org/10.1016/j.mtcomm.2022.104867

17. G. S. Khush, *Plant Mol. Biol.*, **35**, 25-34 (1997). https://doi.org/10.1023/A:1005810616885

18. UN Food and Agriculture Organization, Corporate Statistical Database (FAOSTAT), https://doi.org/10.4060/cb4477en-map13

19. G. Kim, J. Kwak, J. Choi, and K. Park, *J. Agric. Food Chem.*, **60**(3), 718-724 (2012). https://doi.org/10.1021/jf203518f

20. F. Liu, L. Ye, J. Peng, K. Song, T. Shen, C. Zhang, and Y. He, *Sensors*, **18**(3), 705 (2018). https://doi.org/10.3390/s18030705

21. P. Yang, R. Zhou, W. Zhang, R. Yi, S. Tang, L. Guo, Z. Hao, X. Li, Y. Lu, and X. Zeng, *Food Chem.*, **272**, 323-328 (2019). https://doi.org/10.1016/j.foodchem.2018.07.214

22. T.-J. Jiang, Z. Guo, M.-J. Ma, L. Fang, M. Yang, S.-S. Li, J.-H. Liu, N.-J. Zhao, X.-J. Huang, and W.-Q. Liu, *Electrochim. Acta*, **216**, 188-195 (2016). https://doi.org/10.1016/j.electacta.2016.09.016

23. N. Sharma, Kamni, V. K. Singh, S. Kumar, Y. Lee, P. K. Rai, and V. K. Singh, *Appl. Phys. B: Lasers Opt.*, **126**, 122 (2020). https://doi.org/10.1007/s00340-020-07475-8

24. P. Yang, Y. Zhu, X. Yang, J. Li, S. Tang, Z. Hao, L. Guo, X. Li, X. Zeng, and Y. Lu, *J. Cereal Sci.*, **80**, 111-118 (2018). https://doi.org/10.1016/j.jcs.2018.01.007

25. M. Pérez-Rodríguez, P. M. Dirchwolf, T. V. Silva, R. N. Villafañe, J. A. G. Neto, R. G. Pellerano, and E. C. Ferreira, *Food Chem.*, **297**, 124960 (2019). https://doi.org/10.1016/j.foodchem.2019.124960

26. M. Pérez-Rodríguez, P. M. Dirchwolf, T. V. Silva, A. L. Vieira, J. A. G. Neto, R. G. Pellerano, and E. C. Ferreira, *Food Chem.*, **331**, 127051 (2020). https://doi.org/10.1016/j.foodchem.2020.127051

27. P. Yang, R. Zhou, W. Zhang, S. Tang, Z. Hao, X. Li, Y. Lu, and X. Zeng, *Appl. Opt.*, **57**(28), 8297-8302 (2018). https://doi.org/10.1364/AO.57.008297

28. Z. Luo, L. Zhang, T. Chen, M. Liu, J. Chen, H. Zhou, and M. Yao, *Appl. Opt.*, **58**(7), 1631-1638 (2019). https://doi.org/10.1364/AO.58.001631

29. S. H. Choi, J. S. Kim, J. Y. Lee, J. S. Jeon, J. W. Kim, R. E. Russo, J. Gonzalez, J. H. Yoo, K. S. Kim, J. S. Yang, and K. S. Park, *J. Anal. At. Spectrom.*, **29**(7), 1233-1237 (2014). https://doi.org/10.1039/C4JA00069B

30. B.-M. Yao, P. Chen, and G.-X. Sun, *Food Sci. Nutr.*, **8**(2), 982-992 (2020). https://doi.org/10.1002/fsn3.1379

31. G. Jo and T. I. Todorov, *Food Chem.*, **289**, 299-307 (2019). https://doi.org/10.1016/j.foodchem.2019.03.040

32. NIST Atomic Spectra Database, https://www.nist.gov/pml/atomic-spectra-database.

33. U.S. Department of Agriculture, Agricultural Research Service, https://fdc.nal.usda.gov/fdc-app.html#/food-details/168882/nutrients.

34. S. Abdelli-Messaci, T. Kerdja, A. Bendib, and S. Malek, *Spectrochim. Acta Part B: Atom. Spectrosc.*, **60**(7-8), 955-959 (2005). https://doi.org/10.1016/j.sab.2005.07.002

35. D. Choi, Y. Gong, S.-H. Nam, S.-H. Han, J. Yoo, and Y. Lee, *Appl. Spectrosc.*, **68**(2), 198-212 (2014). https://doi.org/10.1366/13-07163

36. S. Wold, M. Sjöström, and L. Eriksson, *Chemom. Intell. Lab. Syst.*, **58**(2), 109-130 (2001). https://doi.org/10.1016/S0169-7439(01)00155-1

Author's Position

Yonghoon Lee : Professor